PINSA, **68, A,** No. 3, May 2002, pp. 293-313

CURRENT HIGH PRESSURE POWDER X-RAY CRYSTALLOGRAPHY

S K SIKKA AND SURINDER M SHARMA

High Pressure Physics Division, Atomic & Condensed Matter Physics Group, Bhabha Atomic Research Centre, Trombay, Mumbai-400 085 (India)

(Received 25 June 2001; Accepted 03 December 2001)

With the availability of powerful synchrotron X-Ray sources and sensitive and fast detectors, X-ray crystallography is now being widely used to solve the problems related to structural variations of materials under high pressures. These studies provide us with the understanding of fundamental mechanisms underlying such changes, and measurements of physical properties for application in various fields. A few typical examples given here elucidate the present international as well as national endeavours in this direction.

Key Words: High Pressure; X-Ray Diffraction; Phase Transitions

1 Introduction

Use of X-ray diffraction for detection and characterization of phase transitions, determination of equations of state and studies for the kinetics of first order phase transitions is now very well established in high pressure science[1,2]. Many exotic crystal structures have been discovered[3]. Some novel phenomena like pressure-induced crystal to amorphous transitions in solids have been the subject of intense investigations in recent past[4]. Equations of state of many materials of importance in applied sciences have been mapped[5]. Many theoretical concepts in the electronic band structure theory of solids, like s-d electron transfer[6] and f electron delocalization[7] etc., have also been verified. X-ray diffraction under high pressures provides vital inputs as well as stringent tests for total energy as well as molecular dynamics calculations. In fact the experiments have helped in bench marking of condensed matter theories so that the latter are now able to make accurate predictions.

All the above have happened because of some revolutionary developments in the experimental technique of X-ray diffraction under pressure. Diamond anvil cell (DAC) in which the sample is subjected to pressure has helped produce Mbar pressure on them in *in-situ* X-ray diffraction experiments[8]. The introduction of area detectors has resulted in reducing diffraction times and in doing more accurate experiments. Solid State detectors made this possible on laboratory sources by energy dispersive X-ray diffraction[9,10]. Now imaging plate phosphors and CCD detectors, along with the advent of synchrotron sources have revived the high resolution angle dispersive technique for pressure studies. In fact, the high pressure community is a major user of synchrotron sources having dedicated high pressure beam lines for their experiments.

In India, there are many groups doing diffraction studies under pressure[11-13]. At BARC, we have been carrying out this for almost two and a half decades. Different type of diamonds anvil cells have been constructed by various groups. However, most of us still employ rotating anode X-ray sources as the 2.5 GeV Indus-2 synchrotron for X-rays is still under construction. Meanwhile many scientific agencies of Government are providing our scientists access to use synchrotron sources in other countries and high pressure researchers in India are beginning to do some experiments on them. In this paper, we will review some of this work. Before we do so, we will first present a brief summary of the X-ray diffraction technique under pressure[14].

2 X-Ray Diffraction in a DAC

Fig. 1 shows a line sketch of the principle of this method. The equipment needed is a source of X-rays, a diamond anvil cell for applying pressure on the sample and a detector to measure the diffracted beam intensity. The sample is put in a sample chamber called gasket. This is squeezed between two diamond pistons for pressure generation. To ensure hydrostatic conditions on the sample, a liquid is also loaded in

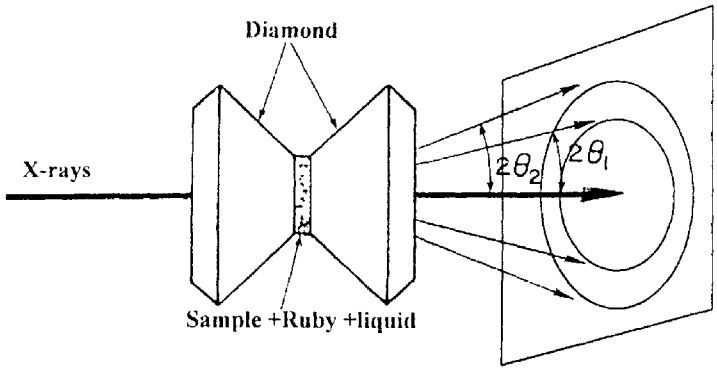

Fig. 1 A schematic of a typical high pressure X-ray diffraction experiment

the gasket along with the sample. Liquids of the type 4:1 mixture of methanol-ethanol freeze at about 10 GPa and the sample environment becomes essentially quasi-hydrostatic beyond this. Noble gas liquids ensure hydrostatic conditions to much higher pressures (~ 70 GPa). Figs. 2 and 3 illustrate the X-ray diffraction set ups and one of the diamond anvil cells used by us at Trombay[15].

As is well known, one can derive the unit cell constants and volume of the cell from Bragg peak

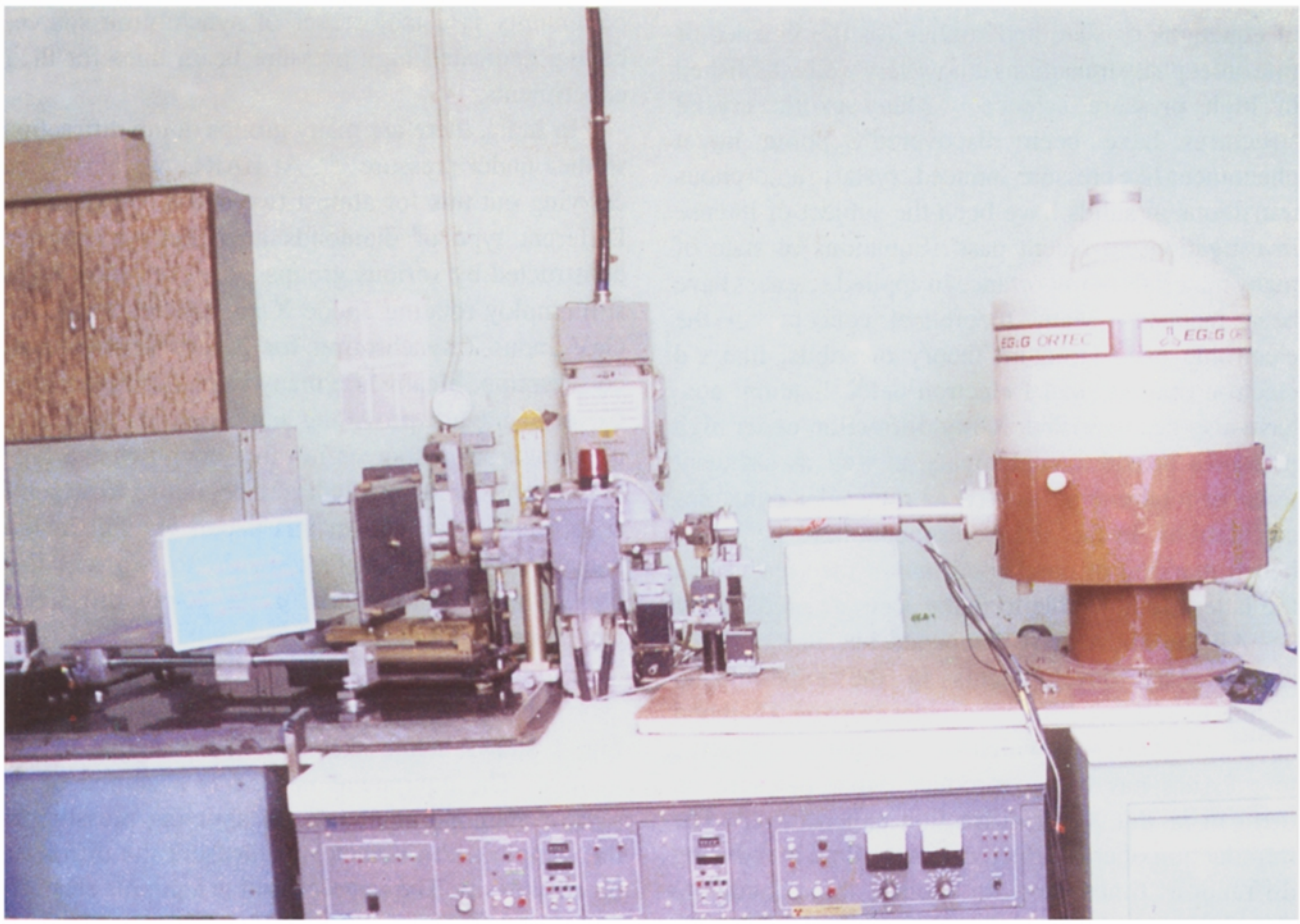

Fig. 2 Experimental set ups at high pressure laboratory at Trombay, BARC for carrying out high pressure powder X-ray diffraction experiments, (a) energy dispersive X-ray diffraction system (right) and angle dispersive set up using imaging plate (left)

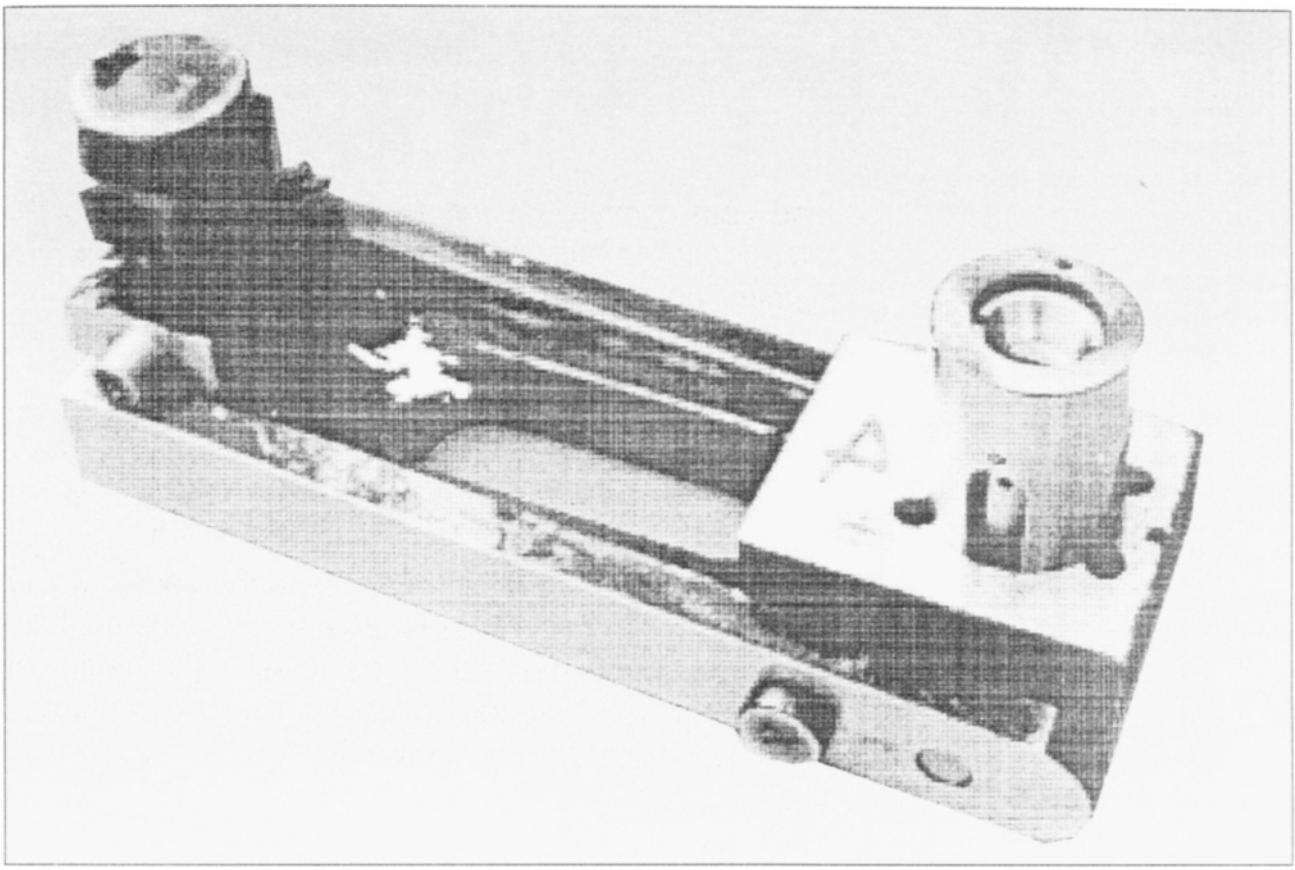

Fig. 3 A Mao-Bell type of diamond anvil cell for X-ray diffraction built at BARC[15]

positions and the unit cell contents from Bragg intensities. Pressure has also to be measured on the sample. For this a pressure marker-usually ruby is also included in the gasket. On shining an appropriate laser beam it emits fluorescence lines R_1 and R_2 (Fig. 4). The frequencies of these lines shift under pressure. This shift is now well calibrated against pressure using P-V data from shock wave experiments. The relative shift of these lines also provides a measure of the non-hydrostatic pressure component.

It is clear from the above simple description that the X-ray diffraction technique under pressure has some inherent limitations compared to room pressure conditions. Both the incident and diffracted X-ray beams have to pass through structural materials of the diamond cell. This restricts the range of the reciprocal space covered. For example, in angle dispersive technique, 2θ is limited to about 50°. Because of the non-uniformity of the pressure across the diamond culets, due to non-hydrostatic pressure component, the Bragg lines broaden and sometimes shift from their true positions under increasing pressure. Thus, the powder patterns are of poorer resolution. Also, because of the uniaxial nature of force applied on diamond pistons, texture invariably develops under pressure. This makes the analysis of intensity data by profile fitting techniques difficult.

Use of synchrotron beams have alleviated to some extent the above problems. Because of the high intensity of these beams one is able to use smaller samples and smaller collimators (~ 5 μm). This means the pressure gradients on samples are smaller. The narrow beams also provide better resolution ($\Delta d/d$ ~ 5 x 10^{-3}). This has allowed investigations of some very subtle phase transitions and of structural mechanisms of phase transitions. This higher intensity has also been helpful in examining kinetics of faster transitions and a look at low Z containing substances and low symmetry structures. In fact, due to the much shorter diffraction times one is able to laser heat the sample in a DAC for *in-situ* P, T phase diagram determination.

3 A CCD Detector for Rotating Anode Based High Pressure Studies

The sample volume inside the gasket in a DAC is ~ 10^{-6}cm^3. Consequently, the exposure time for laboratory X-ray sources is ~ 50 h for film and still

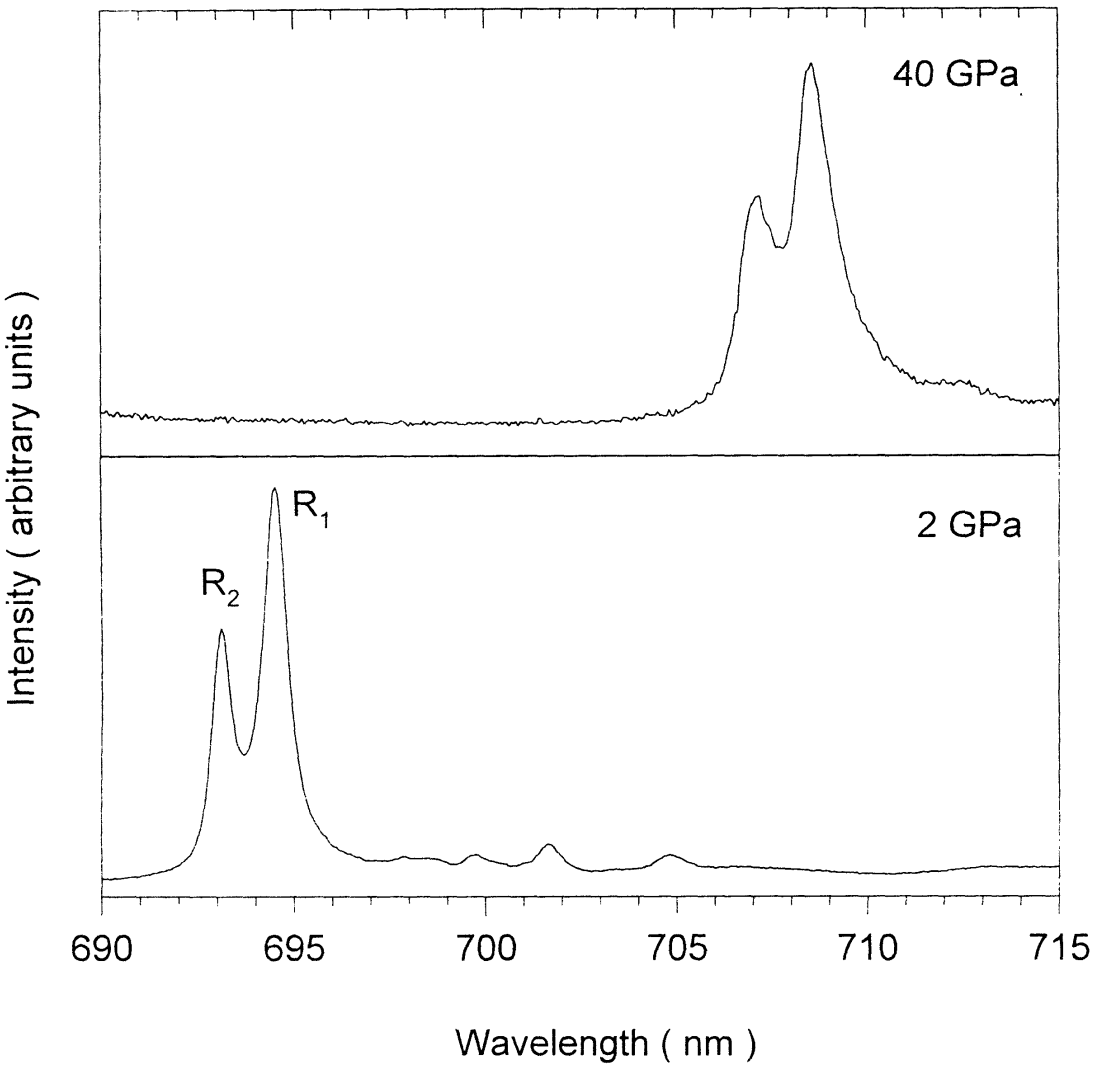

Fig. 4 Ruby R-line fluorescence spectra of a ruby chip in a diamond anvil cell at various pressures

~ 5 h for image plate phosphor detectors. Thus, there is a need for faster detectors. The use of charge-coupled device (CCD) detectors has been suggested but due to lack of adequate size, these have not been used much. To address this, Sinha *et al.*[16] at Trombay have developed a low cost CCD detector of size adequate to cover the 2θ range (~ 40^0) in high pressure experiments. A schematic diagram of this detector is shown in Fig. 5. It consists of a X-ray sensitive scintillator pasted on a fibre optic taper of area 70 mm coupled to a two stage image intensifier tube. The output of image intensifier is transferred through

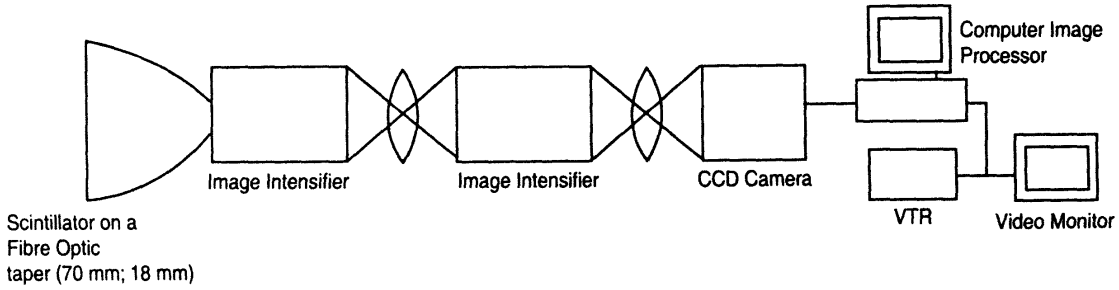

Fig. 5 Schematic diagram of a CCD detector for angle dispersive powder X-ray diffraction made at Trombay[16]

a lens to a CCD imaging camera. These second generation image intensifier tubes have input/output diameter of 18mm with 30 1p/mm spatial resolution. The CCD employed is 1.7 cm in diameter and having 756(H) x 581(V) pixels with pixel size of 11.0 μm(H) x 11.0 μm(V). The video signals obtained from CCD are digitized using a 8 bit frame grabber with a 16 bit processor. The frame grabber has programmable gain amplifier with offset and reference adjustment so that any particular range of gray scale can be zoomed on. This in effect can increase the dynamic range of the system from 8 bit to a higher value depending on combination of gain, offset and reference used. A provision for online thresholding and online dark current subtraction has also been made. Shading correction to account for the systematic non-uniformity of detector response has also been incorporated. The image acquisition system can display real time images on a separate video monitor (each frame time ~ 40ms) or display background subtracted images or integrated images and can also do some preliminary analysis such as measuring intensity profile over a range of pixels in online mode. Two custom designed algorithms have also been developed to analyze the X-ray diffraction patterns. The first one iteratively fits a circle to the diffraction ring in order to determine the pixel position of the centre of the diffraction rings. This technique is also used to correct the tilt of the detector. The second algorithm carries out radial integration along the diffraction rings in order to obtain a better signal to noise ratio in generated one dimensional patterns.

Using the above detector, ambient pressure and high pressure patterns have been collected for many substances. A typical pattern using monochromatic MoKα radiation is shown for La B_6 in Fig. 6 and its one dimensional analog is presented in Fig. 7. The recording time is 30 secs. However, one begins to see diffraction rings emerging in a single frame time of 40 msec time only. One dimensional patterns in a DAC of $In_{0.25}$ $Sn_{0.75}$ alloy in primitive (ph) hexagonal and hexagonal close packed (hcp) phase at 15 GPa are displayed in Fig. 8[16]. Comparison with those recorded by an imaging plate detector (IP)

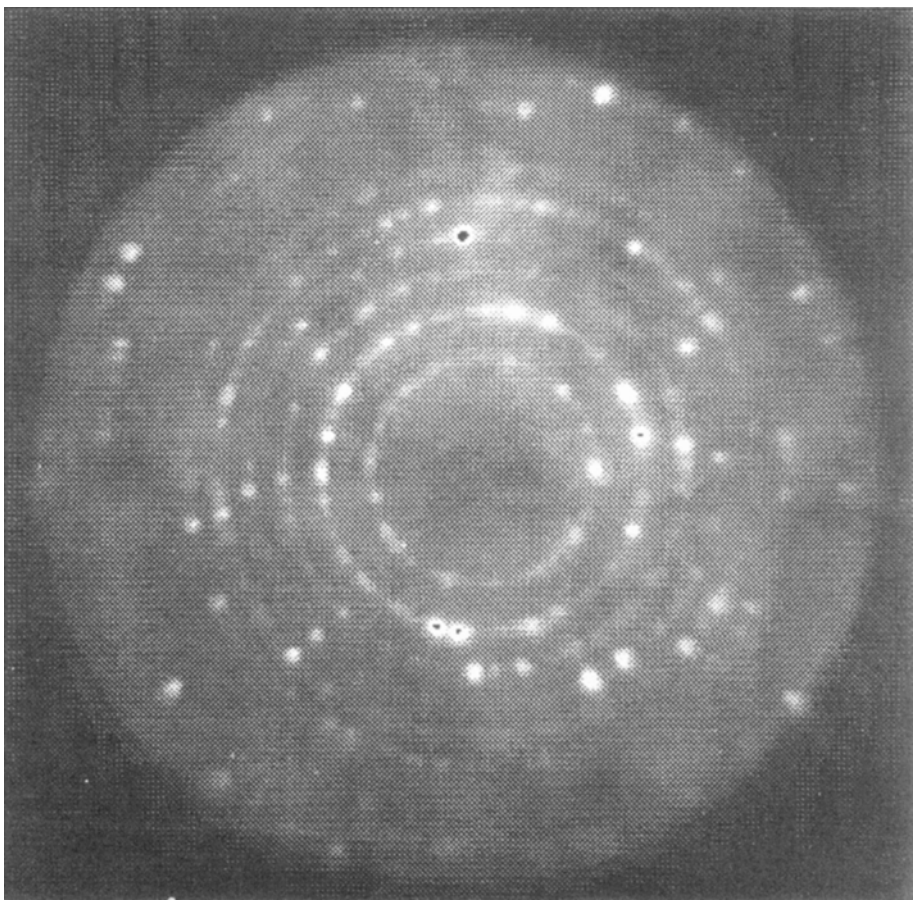

Fig. 6 The diffraction pattern of LaB_6 recorded with the CCD detector

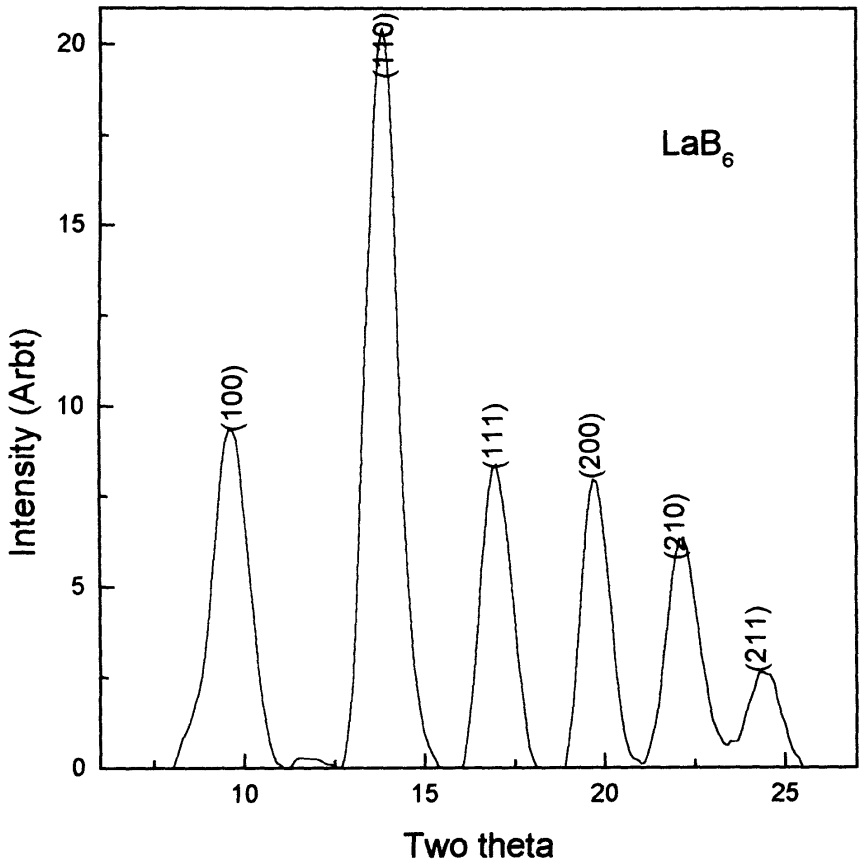

Fig. 7 One dimensional X-ray diffraction profile constructed from Fig. 6

reveals that the unit cell dimensions determined by the detectors are close. However, the resolution because of the pixel size of 170 μm (due to demagnification and scintillator techniques) available for digitizing the patterns was poorer compared to IP. At the present state of development, this CCD detector is found to be extremely useful for quick detection of phase transitions and generation of equation of state data.

4 Pressure Induced Amorphization

The pressure induced crystalline to amorphous (c → a) transition is a topic of considerable current interest (see ref. [4] for a recent review of this field). As is well known, an amorphous phase is characterized by the lack of translational or orientational long range order. Under static pressures more than about 50 substances have now been vitrified. Some of these have also been amorphized using shock loading. In our laboratory this work started with the investigation whose aim was to identify high pressure transitions in $LiKSO_4$. It was noted that beyond a pressure of ~ 12 GPa sharp diffraction peaks of a crystalline phase disappeared (see Fig. 9)[17]. (Normally, a glass should give rise to diffraction pattern similar to that of a liquid. However, as the diffraction intensity goes down drastically on vitrification and as the signal to noise ratio is very poor in a DAC due to scattering from cell materials, the diffraction pattern is completely lost. After this study several other compounds have also been studied.

Molecular dynamics computations (MD) have also been used to understand the structural aspects of this c → a transition[18,19,20]. These have shown that the high pressure amorphous phase has, in most cases, higher cation-anion coordination than the crystalline phase (Fig. 10). In particular it was shown that the structure factor S(Q) in the high pressure amorphous phase and that of fused silica at high pressures are similar[21]. Fig. 11 shows the calculated S(Q) at 28 GPa, 47 GPa and after pressure release (0.1 MPa). The diffraction peaks at 2.15, 3.18 and 4.18 A° at 28 GPa are in complete agreement with the experimental results of Meade *et al.*,[22]. This shift in peaks from

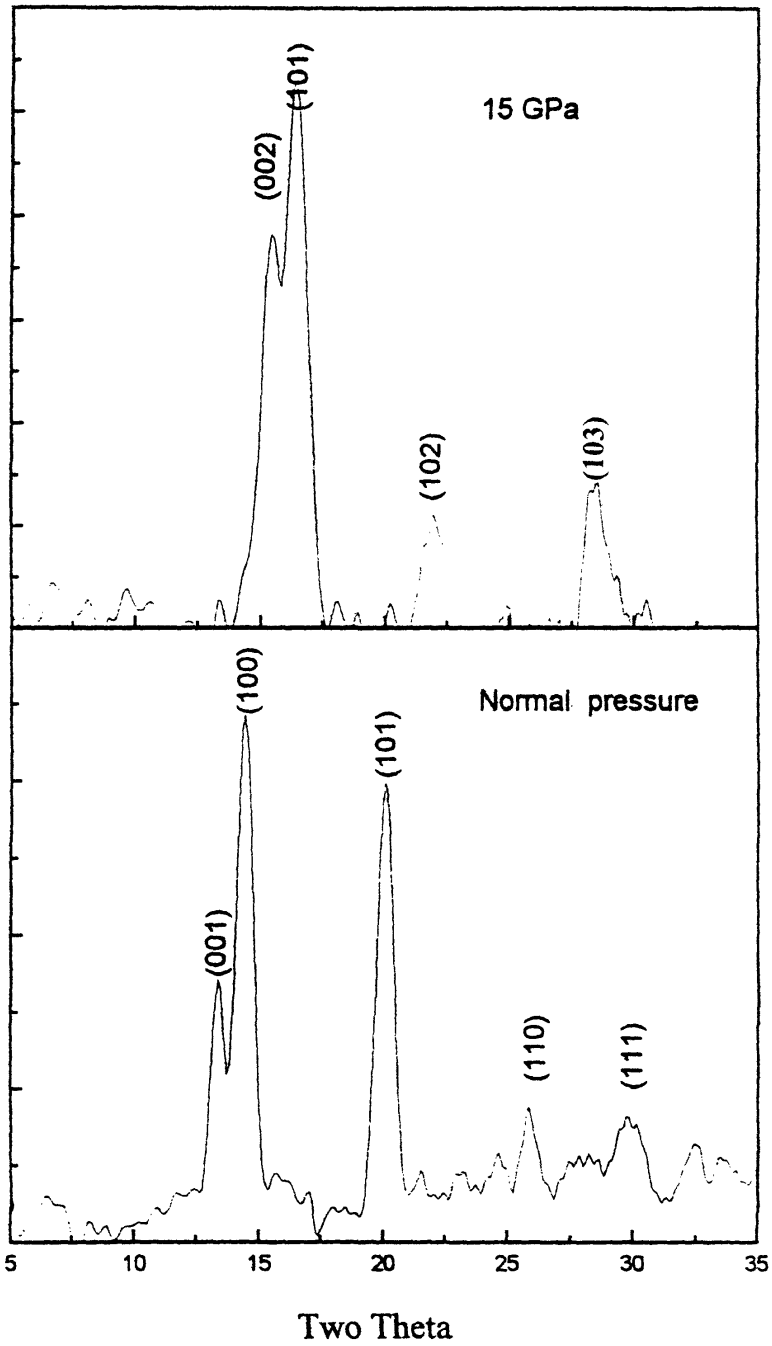

Fig. 8 One dimensional X-ray diffraction of $In_{.25}Sn_{0.75}$ at two pressures, recorded using a CCD based detector

0.1 MPa to new positions is thus related to the change in Si-O coordination from 4 to 6. Essentially the present understanding of these transformations is that the amorphous phase is a kinetically preferred state and can be explained in terms of a three level diagram shown in Fig. 12. Starting crystalline phase is driven to lower its free energy by transformation to a more stable high pressure crystalline phase. However, the amorphous phase is a metastable phase of intermediate free energy. The relaxation times to this metastable phase ($\tau_{c1} \rightarrow_a$) are much shorter than the relaxation times either to stable high pressure phase ($\tau_{c1} \rightarrow_{c2}$) or the relaxation time from amorphous phase to the high pressure structure ($\tau_a \rightarrow_{c2}$). This is due to the fact that high pressure phase has higher coordination

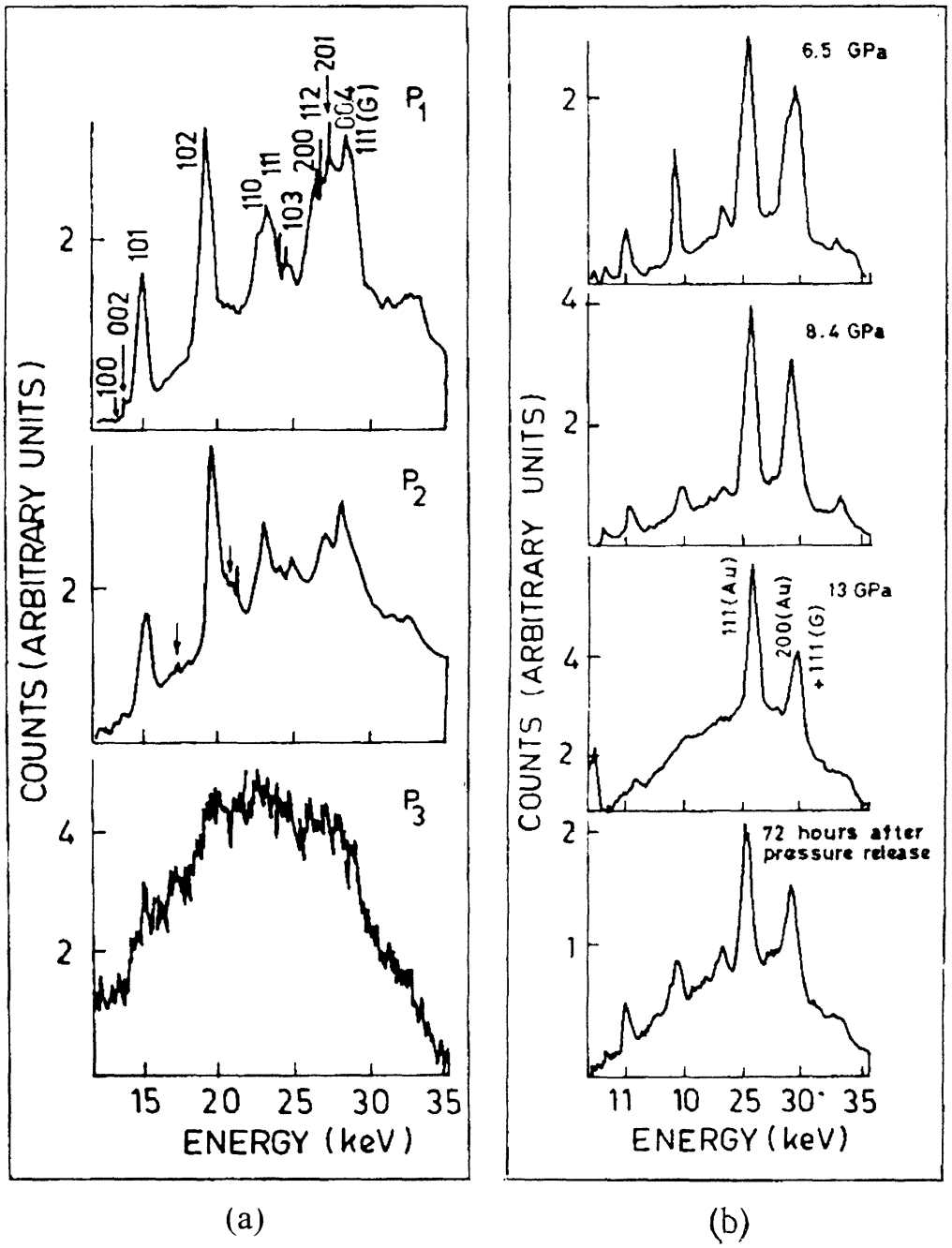

Fig. 9 The loss of diffraction peaks of $LiKSO_4$ on a crystal to amorphous phase transformation. The residual peaks in (b) are due to gold (pressure marker) and gasket

and thermodynamic conditions are not favourable to allow these additional bond formations. The frustration to reach this high pressure ordered structure results in local deformations permitting the necessary coordination change with loss of long range order. In many cases the high pressure stable crystalline phase, access to which is kinetically prohibited, is known by high pressure - high temperature experiments. While in some other cases, where a high pressure crystalline phase is not known, it has been suggested that the stable high pressure phase may be the one in which initial compound has dissociated to smaller and denser constituents.

Structural analysis of most of the materials undergoing these transformations shows that the amorphization sets in when some non-bonded atoms reach their limiting value. For example, in α-SiO_2 the onset of amorphization is brought about when

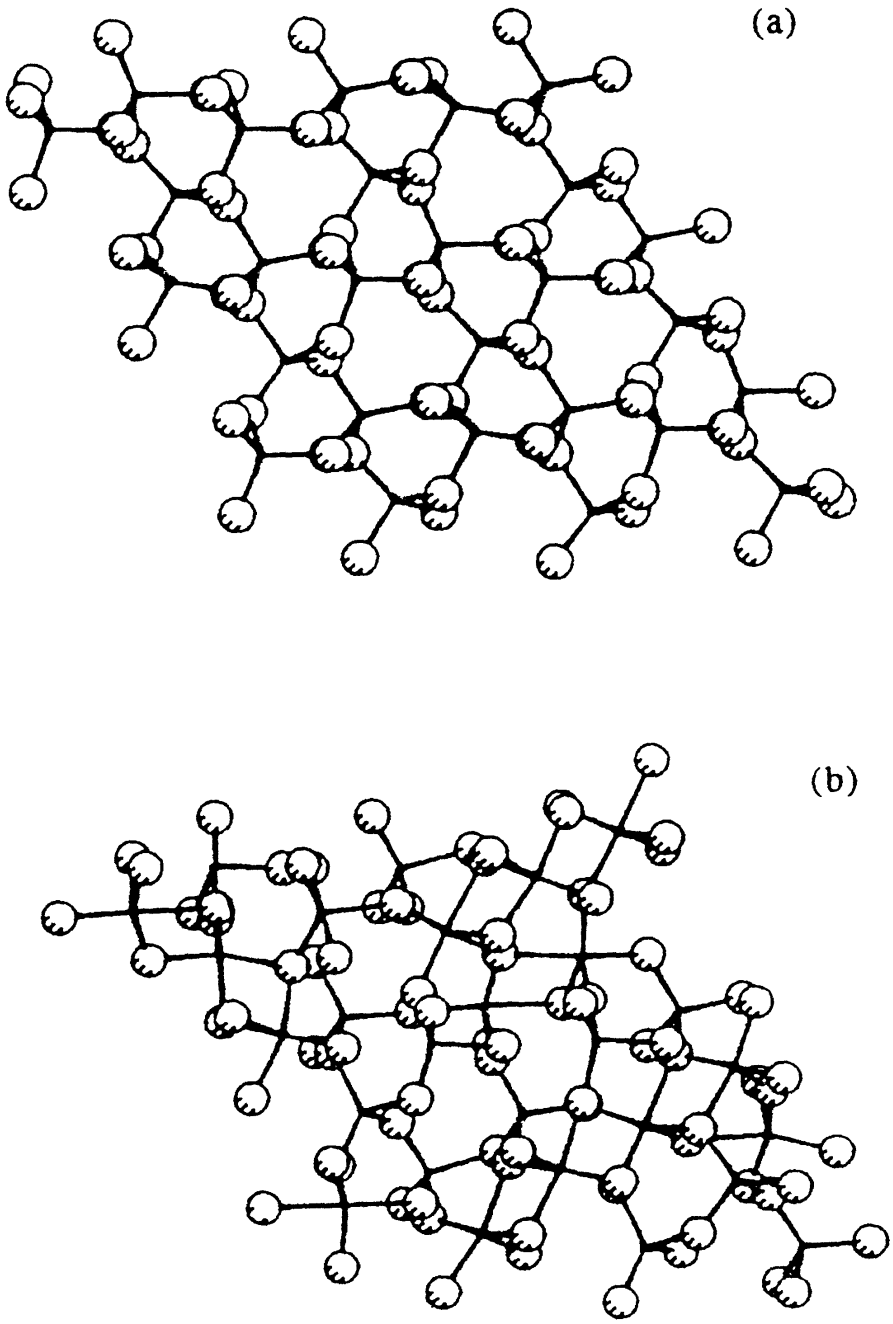

Fig. 10 The structure of α-quartz (a) before and (b) after the amorphization as given by MD simulations[19]

non-bonded O—O distance decreases to 2.8 A[23]. This is related to the fact that at this compression, the increase in the repulsive energy is comparable to typical enthalpy of phase transformations. The reversibility, wherever observed, has been ascribed to non-deformability of some constituent species in the structure. For example in $LiKSO_4$ this may be due to the fact the SO_4 tetrahedra do not deform much while in $AlPO_4$, PO_4 tetrahedra remain substantially undistorted.

5 α- $AlPO_4$: Is It a Memory Glass ?

For over a decade, berlinite, $AlPO_4$ (Fig. 13) has been known to be a memory glass i.e. on pressure release, the high pressure amorphous phase reverts back to the initial single crystal with same orientation. Earlier experiments[24,25] as well as molecular dynamics calculations (MD)[18] had claimed that berlinite amorphizes at 15 GPa (experiments) or 30 GPa (MD). However subsequent Raman scattering studies by Gillet *et al.*,[26] and MD calculations[5] raised doubts

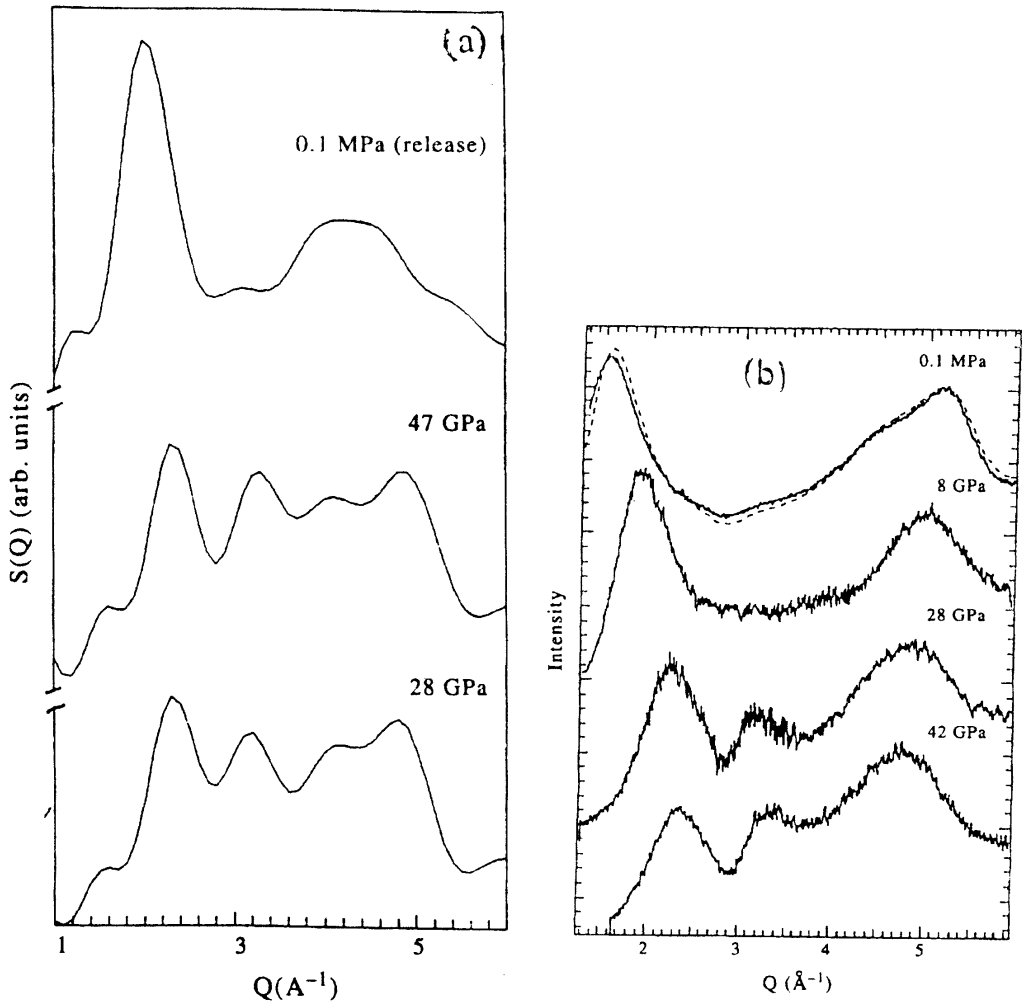

Fig. 11 Comparison of calculated S(Q) for a pressure induced glass with experimental S(Q) of fused silica[22]

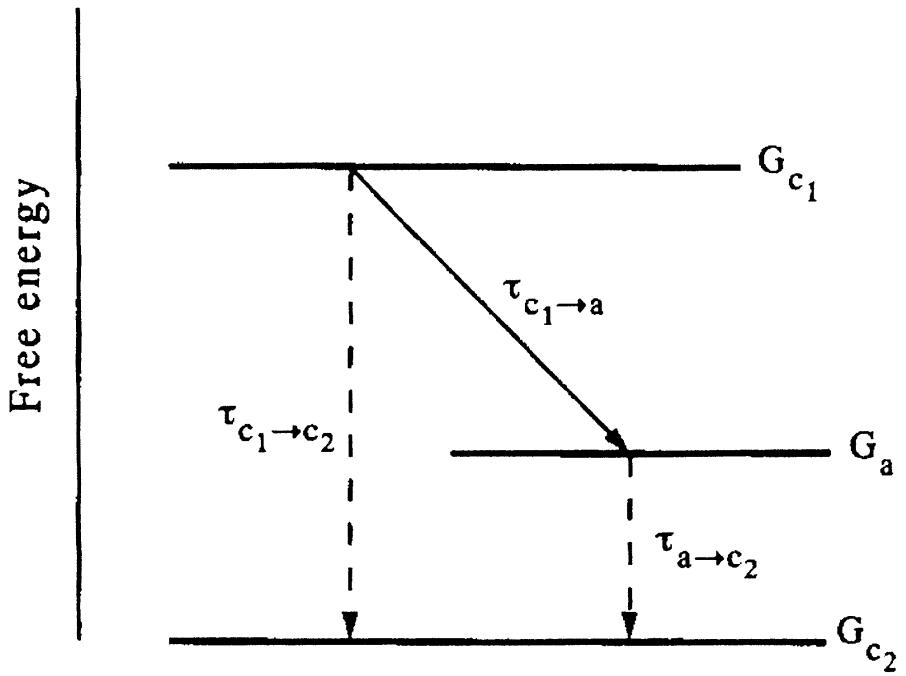

Fig. 12 A schematic three level diagram for crystalline to amorphous (c® a) transformation

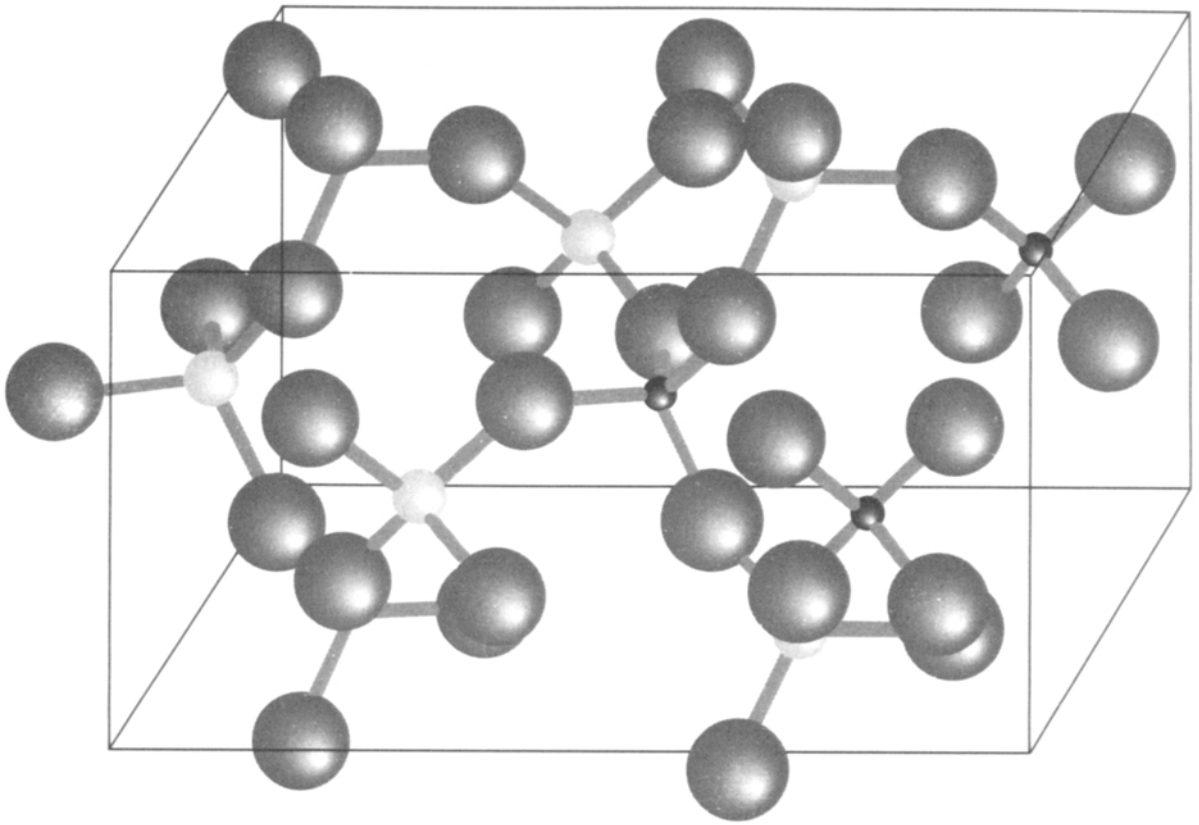

Fig. 13 The ambient structure of berlinite (a- $AlPO_4$). Dark black spheres are phosphorus atoms while light gray one represent Al atoms. Oxygen atoms are shown by the largest size

on these earlier studies. Gillet *et al.*, reported emergence of new Raman bands at around 14 GPa suggesting a crystalline to crystalline phase transition. Recent MD studies indicated that there could be a disorder in the oxygen sublattice for P ≥ 15 GPa, which will show up in the reduction of the intensity of calculated diffraction peaks. In addition, these calculations also showed that though berlinite undergoes a first order phase transition at 30 GPa, in agreement with earlier calculations, it does not become X-ray amorphous till 65 GPa[23]. To clarify these issues X-ray diffraction experiments were carried out on α-$AlPO_4$ at the beamline BL10XU of SPring –8 by Sharma *et al.*,[27]. These experiments (Fig. 14) revealed a crystal to crystal phase transition near 13 GPa. In addition, a systematic overall increase in the background was also observed indicating some kind of disorder. Profile fitting analysis of these diffraction patterns showed that the new phase at 13 GPa had an $InPO_4$ structure in the Cmcm space group. This structure is shown in Fig. 15. In this Cmcm structure which is regarded as the equilibrium phase at high pressures of this material (see last section), Al and P are six and four coordinated to the nearest oxygen atoms respectively. This structure was shown to be thermodynamically more favourable than the α-phase above 12 GPa, though classical molecular dynamics calculations failed to access this phase. The existence of increased background along with new diffraction peaks characteristic of Cmcm phase suggests that the new structure is a disordered Cmcm phase, much like what is seen in recent MD calculations of cristobalite[28].

On release of pressure the initial alpha phase is retrieved with no signatures of any remnant Cmcm phase. Fig. 16 shows the P-V curve determined from these experiments. A fit to Murnaghan equation to the berlinite data gives the bulk modulus, K = 34.0 and K_0' = 4. In comparison, Cmcm phase is found to quite incompressible with K = 127 with K_0' =4. The c/a for the berlinite phase increases smoothly and is in disagreement with MD predictions. It was also found that berlinite $AlPO_4$ does not fully amorphize upto 40 GPa, which disproves earlier experimental as well as theoretical results. Due to the existence of a crystalline-crystalline phase transition observed here, it is more likely that the so called memory glass effect may be due to the reversibility of α-$AlPO_4$ ⇔ Cmcm phase transition. These new results should encourage fresh theoretical work on this problem.

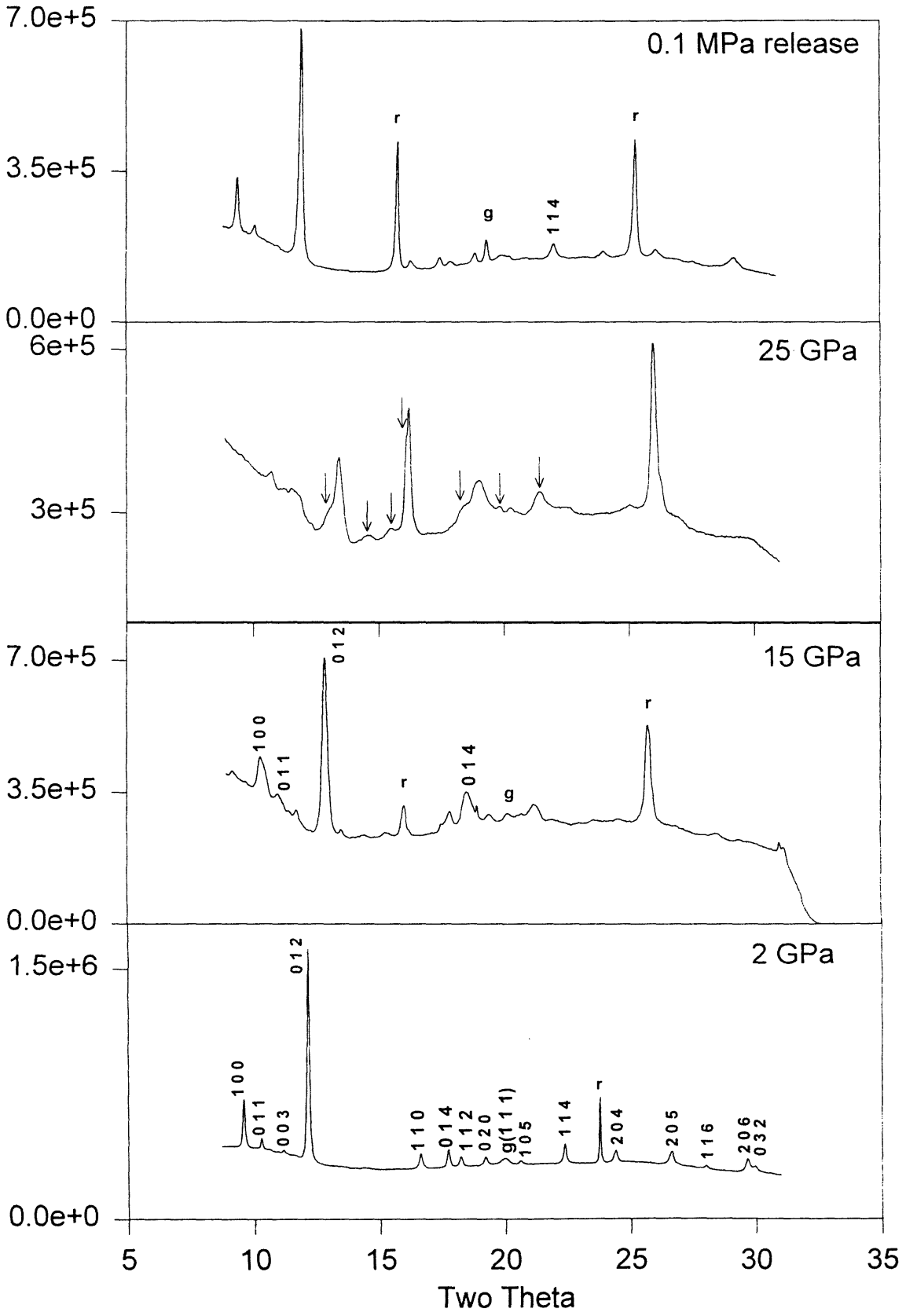

Fig. 14 X-ray diffraction of $AlPO_4$ at various pressures. New peaks of Cmcm phase are marked with arrows at 25 GPa

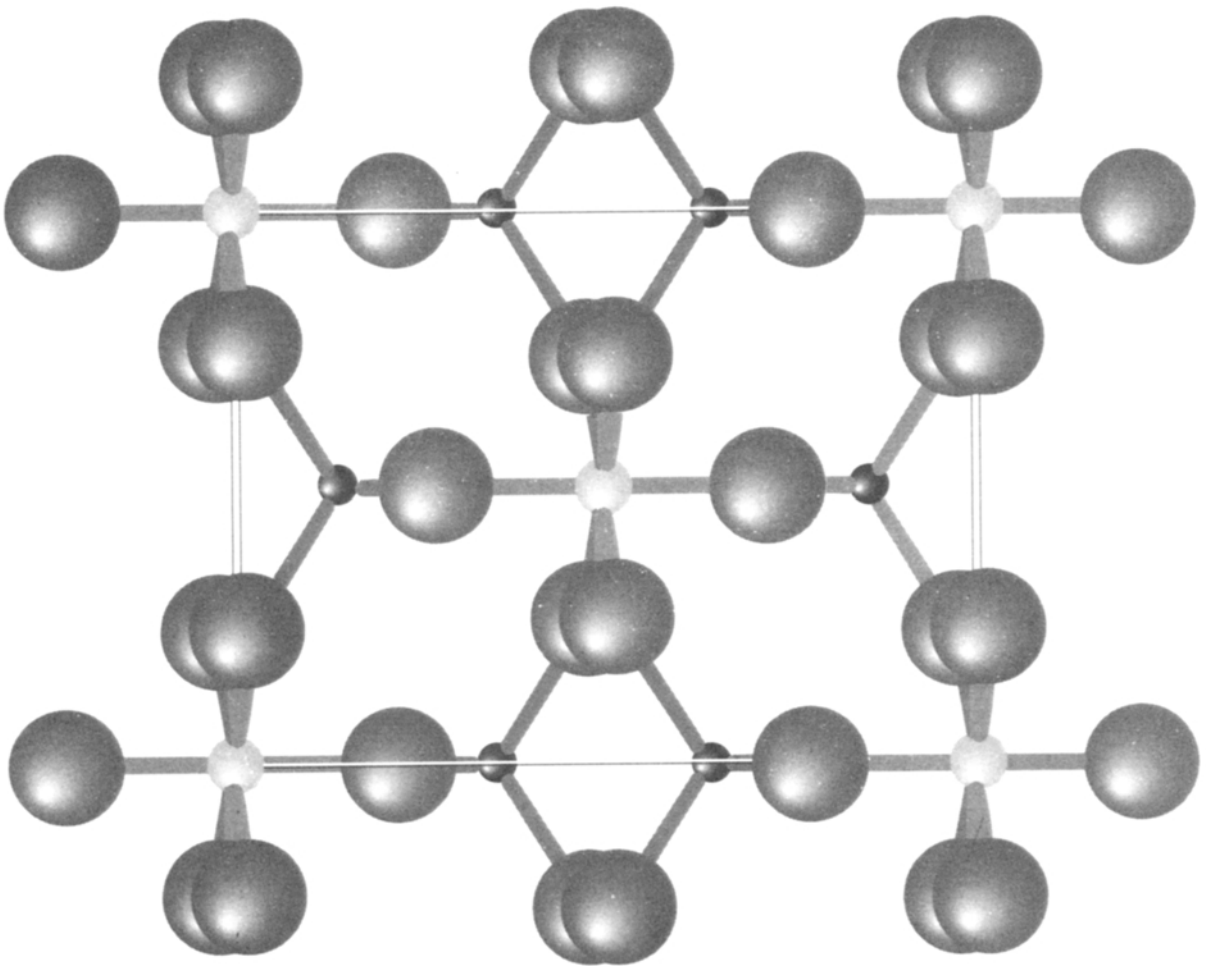

Fig. 15 Proposed new structure (Cmcm) of $AlPO_4$ at high pressures. Al-O coordination. increases to six while P-O continue to be tetrahedrally connected in this structure. (Atomic notation same as in Fig. 13)

6 High Pressure Phase Transitions in Admantane - $C_{10}H_{16}$

It was pointed out in Section 2, that one major advantage offered by the high intensity of synchrotron X-ray beams is to make the high pressure X-ray diffraction measurements possible on low Z containing compounds. Here outstanding applications are hydrogen upto 120 GPa[29] and ice upto 210 GPa[30]. The latter study indirectly confirms that the hydrogen bond in it becomes symmetric at 60 GPa, as revealed by infra-red experiments. Here, we describe an investigation on admantane, $C_{10}H_{16}$. At ambient conditions, this crystallizes in an orientationally disordered cubic structure (space group F m3m with Z = 4), usually referred to as a plastic phase[31]. This transforms to an ordered tetragonal phase (P4 2_1 c, Z = 2) below 208 K or above 0.5 GPa[32]. In these structures, the globular admantane molecules are held together by van der Waals forces. At 0.1 MPa shortest contacts are non-bonded H—H separations with a value of ~ 2.4 A. Under compression, these should decrease and become repulsive and lead to the breakdown of parent structure and new phases. In fact, the phase transition at 0.5 GPa may be rationalized in the above framework. The tilting of admantane molecules

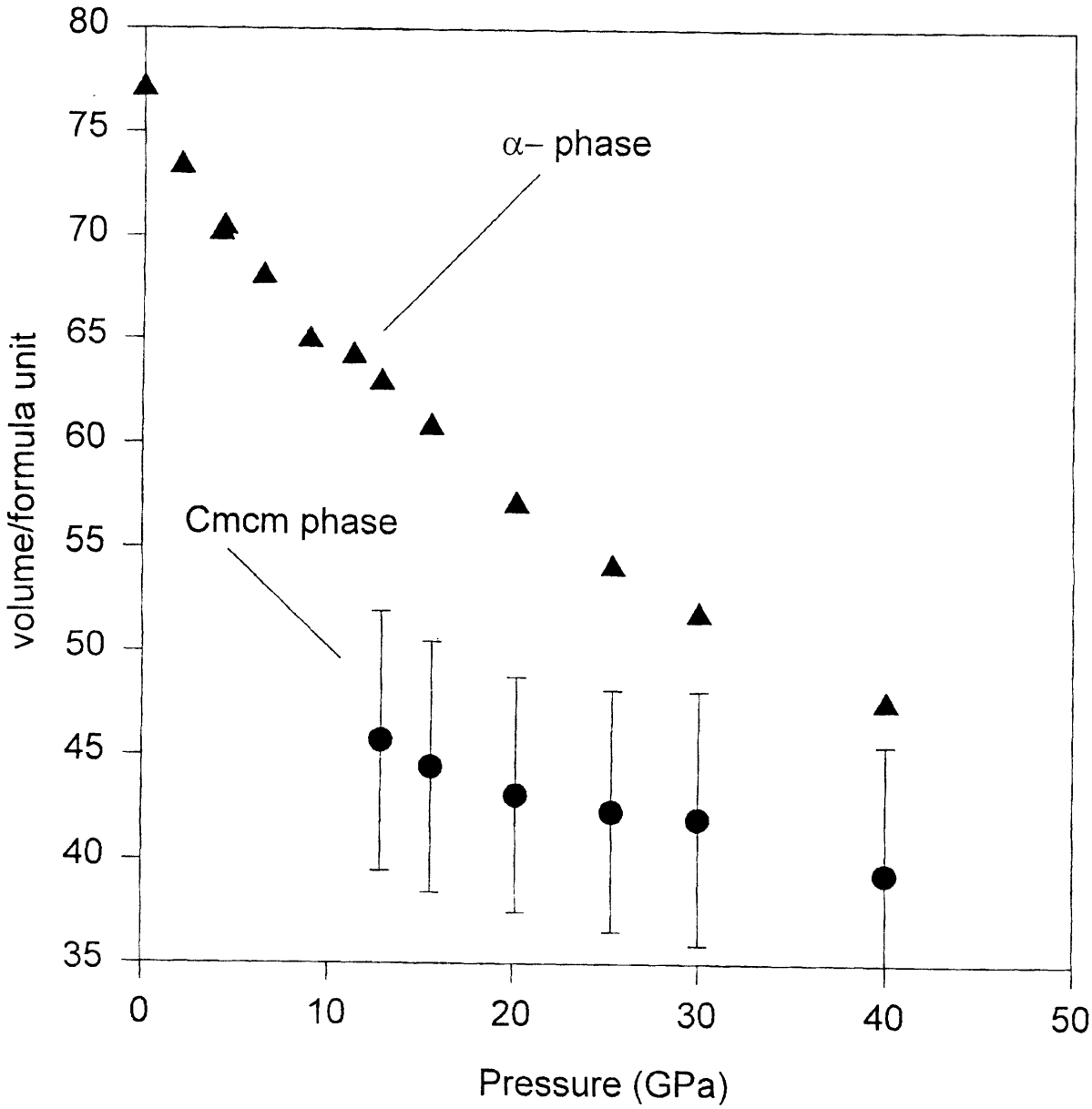

Fig. 16 Pressure volume curve of $AlPO_4$ of *a* and Cmcm phases

in the P4 2_1 c structure is a consequence of the increased H—H repulsion and is an attempt by the crystal to relieve this. The H—H distances which are ~ 2.2 A^0 just before the phase transition become larger after this transition.

Further compression should lead to new structures or amorphisation when H—H contacts attain limiting values of ~ 2A[33]. Raman studies done at Trombay on admantane have identified more phase changes at 2.5, 8.5 and 18-23 GPa respectively[34]. In order to confirm the above, Vijayakumar *et al.*,[35] have carried out angle X-ray diffraction measurements on admantane upto 25 GPa at the BL10XU beam line of the synchrotron source SPRING-8. Because of low scattering power of X-rays by atoms in $C_{10}H_{16}$, the diffraction time for each pressure was about three hours compared to half an hour for $AlPO_4$ (see section 5). Diffraction patterns of admantane at some pressures are shown in Fig. 17. These indicate that changes occur at 0.5, 2.5, 9 and 19 GPa in agreement with Raman results. The phase above 0.6 GPa is the P4 2_1 c one. Preliminary Reitveld refinement by constraining the inter atomic bond distances and bond angle within a narrow range in the admantane molecule, show that H—H distances reach 2.05 A^0 at 9 GPa where another change in diffraction pattern is experimentally observed. Detailed analysis will be reported elsewhere.

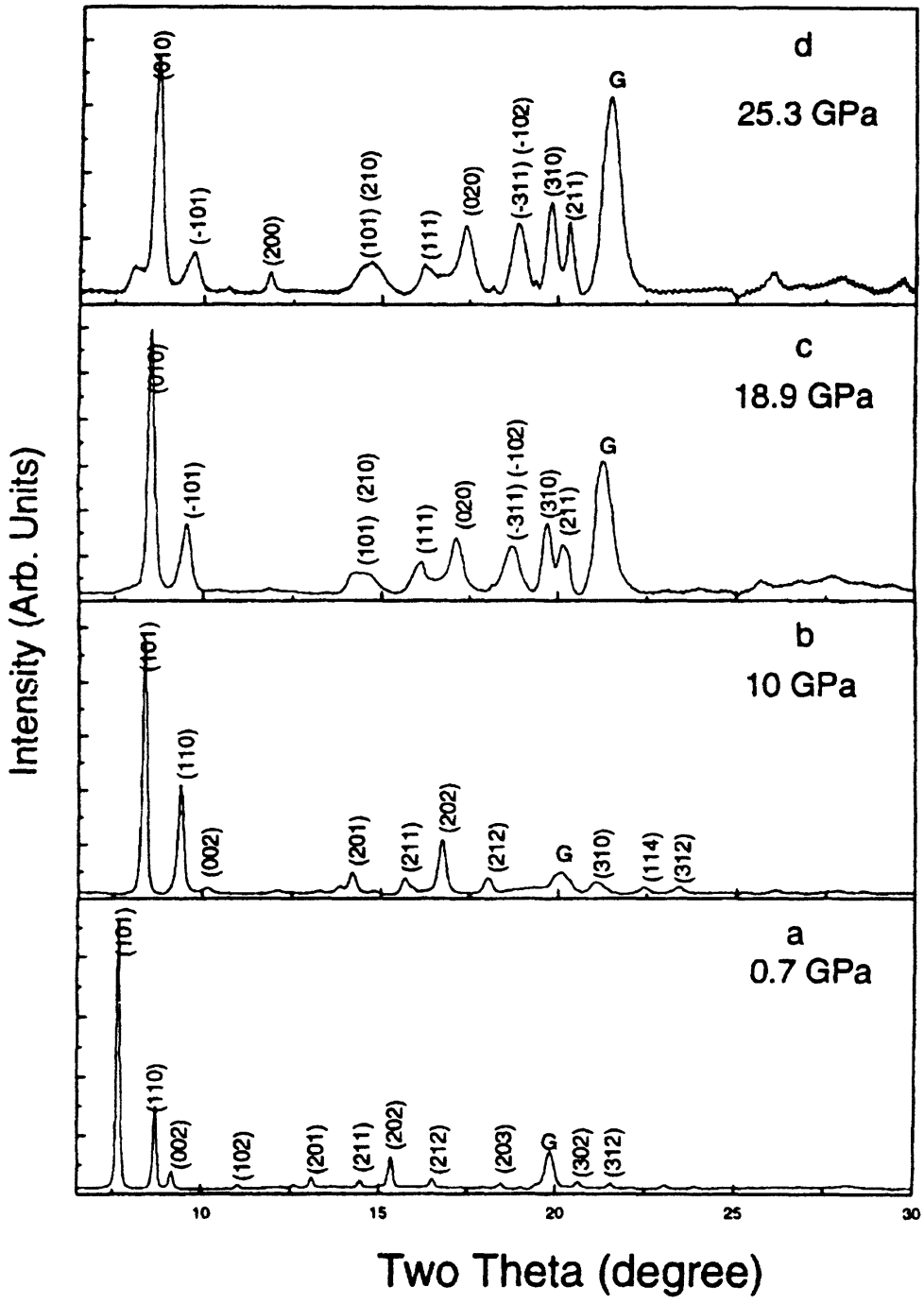

Fig. 17 X-ray diffraction patterns of adamantene at different pressures. Patterns upto 18.9 Gpa indexed on $P42_{1c}$ and other tetragonal cells. The ones at 25.3 Gpa is for monoclinic structure[35]

7 Determination of Crystal Structures through Molecular Dynamics Computations

As pointed out earlier, the X-ray diffraction data available from the high pressure experiments is limited (d = 1 – 5A) and thus there may be a few diffraction peaks available in the pattern. This puts severe constraints for determining the new structure by usual techniques. Generally one uses either the knowledge of phase diagrams of related and similar compounds, or empirical homology rule which states that compression and chemical substitution by an element with a higher atomic number generally result in same structural trends. Sometimes symmetry considerations are also employed because most of the high pressure phase changes are displacive or martensitic[36]. In a pioneering study at Trombay[21], it

was shown that molecular dynamics calculations can also be very effectively used for identifying new structures. Experimental studies on α-quartz showed that at 21 GPa, prior to amorphization, this compound undergoes a crystalline to crystalline transformation[37]. Somayazulu *et al.*, simulated the high pressure behaviour of α-quartz using molecular dynamics calculations with reliable pair potentials of Tsuneyuki *et al.*,[38]. The calculated diffraction pattern at 21 GPa from the atomic coordinates of the structures thus generated agreed with the experimental results. A triclinic cell with a = 3.87°, b = 4.31°, c= 5.11 A°, α = 83.2°, β = 83.8° and γ = 117.4° was able to explain most of the observed diffraction peaks. Fig. 18 (Table I) shows a comparison of the observed and calculated d-spacing as a function of pressure. Since after these calculations various investigators have routinely used this method to determine the structure of the high pressure phases.

Table I

Calculated d-spacings at GPa, and their indices with respect to the MD unit cell of α-quartz, which gets distorted to a = 3.87Å, b = 4.31Å, c=5.11 Å, α = 83.2°, β = 83.8° and γ = 117.4° at this pressure[21]

d(Å)	(h k l)	d(Å)	(h k l)
3.775	1 0 0	2.034	1 0 2
3.674	$\frac{2}{3}\ \frac{\bar{2}}{3}\ 1$	1.970	$\frac{4}{3}\ \frac{\bar{2}}{3}\ 2$
2.788	1 0 1	1.922	0 2 0
		1.720	0 2 1
2.664	$\frac{4}{3}\ \frac{\bar{2}}{3}\ 1$	1.626	$\frac{1}{3}\ \frac{5}{3}\ 2$
2.557	$\frac{1}{3}\ \frac{1}{3}\ 2$	1.485	$\frac{5}{3}\ \frac{2}{3}\ 1$
		1.445	0 2 2
2.398	$1\ \frac{2}{3}\ 1$	1.388	1 1 3
2.254	$\frac{1}{3}\ \frac{4}{3}\ 1$	1.312	2 1 2

8 Determination of Single Crystal Elastic Modulii at Mbar Pressures

Determination of the elastic constants is important for understanding the bonding characteristics of solids under different deformation conditions and also has important applications in metallurgy and seismic wave propagation in earth. So far these elements of the elasticity tensor could be measured to very low pressures (~ 3 GPa) using ultrasonic techniques and by Brillouin spectroscopy for transparent samples to moderate pressures (< 20 GPa). Recently, A K Singh from National Aerospace Laboratories, (India) alongwith his collaborators from Geophysics Laboratory in Washington DC[39,40], have employed X-ray diffraction on polycrystalline samples under non-hydrostatic compression to derive the elastic constants. The basis of the technique is as follows.

The stress state on sample compressed between two anvils can be split into hydrostatic pressure

$$\sigma_p = (\sigma_3 + 2\sigma_1)/3$$

and a deveatoric stress

$$t = \sigma_3 - \sigma_1$$

where σ_1 and σ_3 are the radial and axial stresses respectively. Singh has shown that for all crystal systems a given d spacing is related to the angle Ψ between the diffracting plane normal and the load axis by

$$d(hkl) = d_p(hkl)\ (1+(1-3\ \cos^2\Psi)\ Q(hkl)$$

Here d_p is the d spacing under hydrostatic pressure and Q(h kl) is the lattice strain under the uniaxial stress condition

$$Q\ (hkl) = (t/3)\ [\alpha\{2G_R(h\ kl)\}^{-1}+(1-\alpha)\ (2G_V)^{-1}]$$

and is related to elastic constants. Here G_R and G_V are shear modulii under isostress and isostrain conditions. Detailed expressions have been derived by Singh[41]. Using the synchrotron diffraction data measured at different values of angle ψ in a specially designed DAC, Mao *et al.*[40] have determined elastic constants for many materials to Mbar pressures. To create non-hydrostatic conditions no pressure medium was added in the DAC. In particular, Table II shows a comparison of these with theoretical band structure calculations for hcp Fe. The agreement is quite impressive.

Table II

Elasticity of hcp Fe (from Mao et al.[40]*)*

	39 GPa		211 GPa	
	Exp.	Theory	Exp.	Theory
P	9.67	10.09	12.61	12.80
C_{11}	604	747	1303	1697
C_{12}	244	301	637	809
C_{33}	493	802	1302	1799
C_{13}	254	297	637	757
C_{44}	271	215	960	421
K	351	455	1071	1085
G	134	224	396	446
V_P	6.84	7.86	10.42	10.54
V_S	3.76	4.72	5.61	5.90

ρ is gm cm^{-3}, C_{11} to G are in GPa and V_p & V_s are in kms^{-1}

9 Stability of the Pressure-Induced Orthorhomic Phase of Iron

The phase diagram of iron at high pressures and high temperatures is of considerable importance in geophysics. The Earth's core consists of two layers: the solid inner layer and the liquid outer layer containing mostly iron mixed with a small proportion of lighter elements like S, O, H, Si, Mg, etc.[40] Until recently iron has been known to occur in four solid phases: α(bcc) which is magnetic, δ(bcc) which is non-magnetic, γ(fcc), and ε (hcp). In 1993, Saxena and co-workers[43,44] discovered a new iron phase between 30-60 GPa in samples quenched from the temperature range 1500-2200 K. They called it β phase and indexed the diffraction pattern of this phase on a double hexagonal-close-packed (dhcp) structure. Almost at the same time, Yoo *et al.*[45] observed the dhcp structure below 40 GPa at high temperatures by *in situ* X-ray diffraction. However, at higher pressures iron continued to be hexagonal-close-packed in their experiments.

Andrault *et al.*[46] recently carried out angle-dispersive X-ray diffraction measurements of iron in a laser-heated diamond-anvil cell up to 2375 K and in the range of 30-100 GPa pressures. The data were collected to larger 2θ angles using the image plates as detectors. This investigation revealed that iron undergoes a phase transformation at high pressures and temperatures to an orthorhombic structure (in Pbcm space group). This orthorhombic structure can be described as distortions of the fcc and hcp lattices.

To evaluate the stability of this new phase, Rao *et al.*[47] carried out first principles electronic total energy calculations. They evaluated total energies by the scalar relativistic linear muffin-tin orbital method within the atomic-sphere approximation[10-12]. The exchange-correlation terms were considered by the Perdew-Burke-Ernzerhof form of the generalized gradient approximation. The s, p, d, and f components for the angular momentum expansion of the electron orbitals were included. Electronic structure calculations in the fcc, hcp, dhcp, and orthorhombic structures were done at seven values of compressions in the range from 0.5 - 1.0 for V/V_0 (V_0 being the ambient volume).

These calculations showed that the total energies of the fcc and the dhcp structures are close to each other (within 1 mRy/atom), and 6-8 mRy above that of hcp. The orthorhombic phase, however, is 40-55 mRy/atom (Fig. 18) higher in energy. The entropy energy difference between the orthorhombic and hcp structures was estimated to be ≅ 2 mRy/atom at 2200 K. Thus the experimental observation of the orthorhombic structure by Andrault *et al.* is not supported by these results. It may, however, be possible that due to thermal fluctuations, the intermediate orthorhombic structure may be stabilized. But, in the recent energy dispersive experiments[48] with a doublesided laser-heated diamond-anvil cell for avoiding the thermal gradients, no solid phase other than ε-Fe (hcp), and γ-Fe (fcc) was observed *in situ* at high temperatures (> 1000 K) and pressures up to 84 GPa.

This is an example where the theory is able to disapprove a structural interpretation of the high pressure X-ray diffraction data.

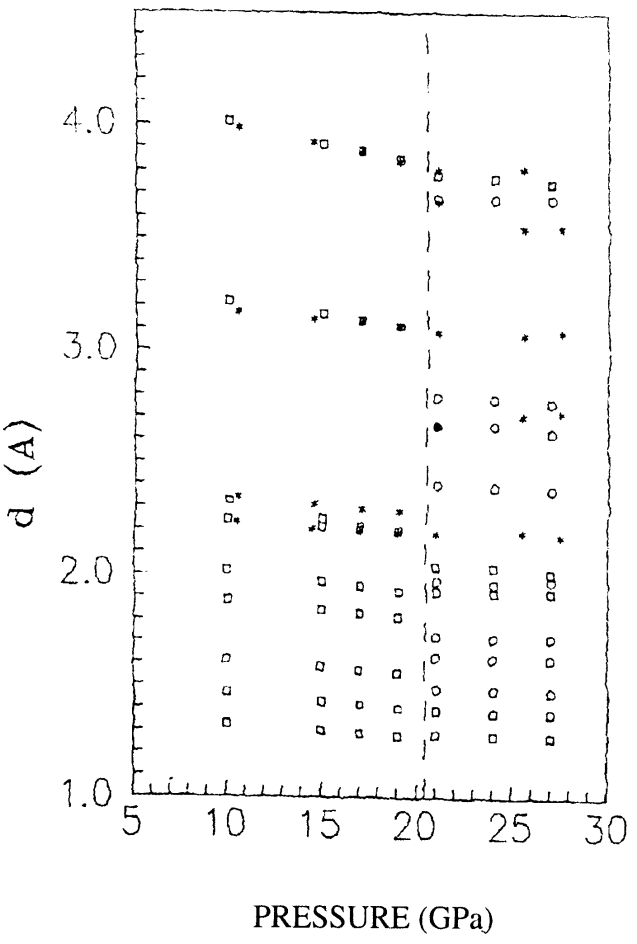

Fig. 18 Comparison of calculated and observed variation of the d spacing of the diffraction lines in the range of 1-5 A as a function of pressure. represents the calculated d values for a-quartz while non-quartz like peaks are shown by o. * denotes the experimental data of Kingma *et al.*[37]

10 High Pressure Phases of Si

On increasing pressure Si shows the following structural sequence : diamond phase (12 GPa) → β tin phase (16 GPa) → ph (38 GPa) → Si VI (42 GPa) → hcp (78 GPa) → fcc[3,49]. Here ph is the simple-hexagonal structure, observed for the first time in an elemental system. Later on this phase was found in Ge, again on transformation from the β - Sn structure[50]. These experimental studies stimulated a large number of theoretical investigations. These concerned the relative stability of various structures through band structure based total energy calculations and also about the mechanisms of transformations. In particular, Sharma and Sikka[51] postulated that the transformation between β - Sn and ph phases should take place through an intermediate orthorhombic phase which is a subgroup of both β - Sn ($I4_1/amd$) and ph (P6/mmm) structures. Fig. 20 shows this transformation mechanism. Moving the two bct sublattices in the β - Sn structure towards the other, one gets an orthorhombic structure which can be either body centred (larger cell) or base centred cell. This may be then transformed to the ph structure by rearrangement of axis. An exact ph structure would be obtained if c/a for β - Sn is $\sqrt{\frac{1}{3}} = 0.58$, instead of the real value of 0.54. Thus, both shuffles of atoms and small homogeneous distortions are necessary.

Taking advantage of the high resolution data from angle dispersive diffraction set up at Daresbury Synchrotron, McMahon and Nelmes[52] observed this intermediate phase at 13 GPa (Fig. 21). Systematic absences were consistent with Imma or Im2a space groups. Rietveld refinement of the trial structure with atoms at 4(e) positions of Imma, (0, ¼, z) gave z = 0.193 with unit cell dimensions of a = 4.737, b = 4.502 and c = 2.558. This means that the atoms of the second body centred lattice in β - Sn at 13 GPa have not yet moved by the full translation along

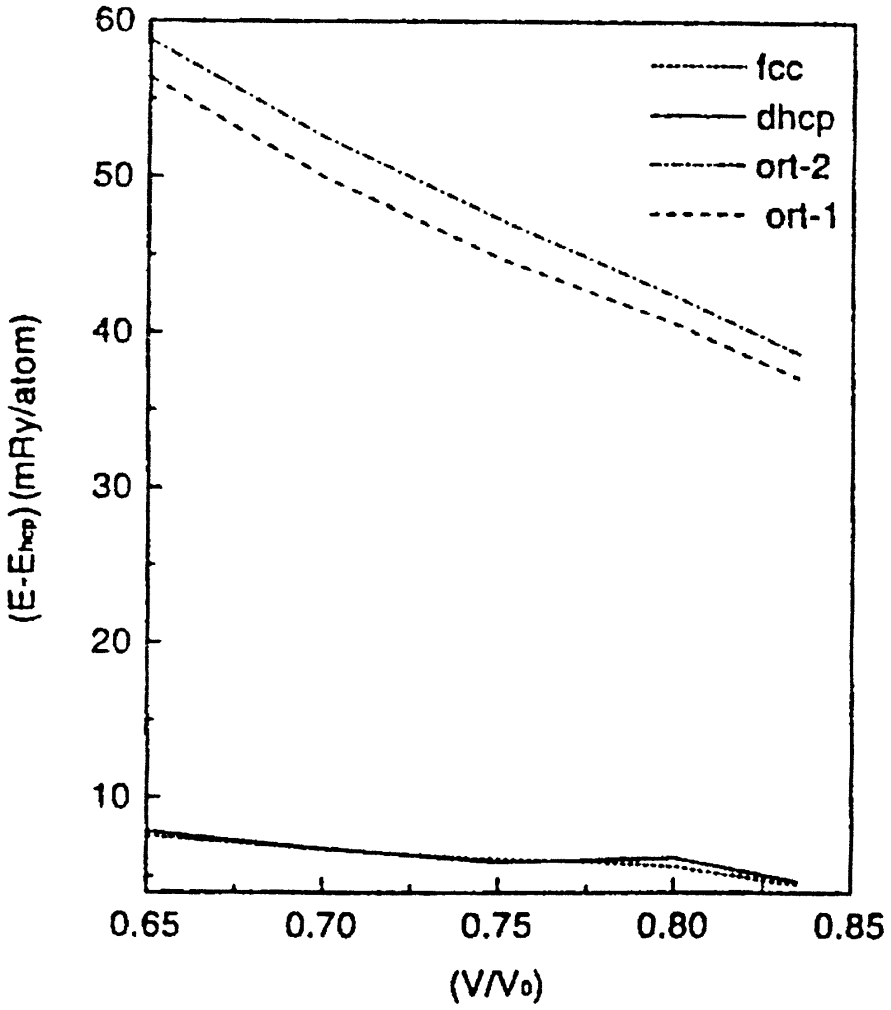

Fig. 19 Variation of total energy of iron with compression (with respect to the energy in the hcp structure). The curve marked ort-1 corresponds to the proposed orthorhombic structure at 44.6 GPa and ort-2 that at 100 GPa[46]

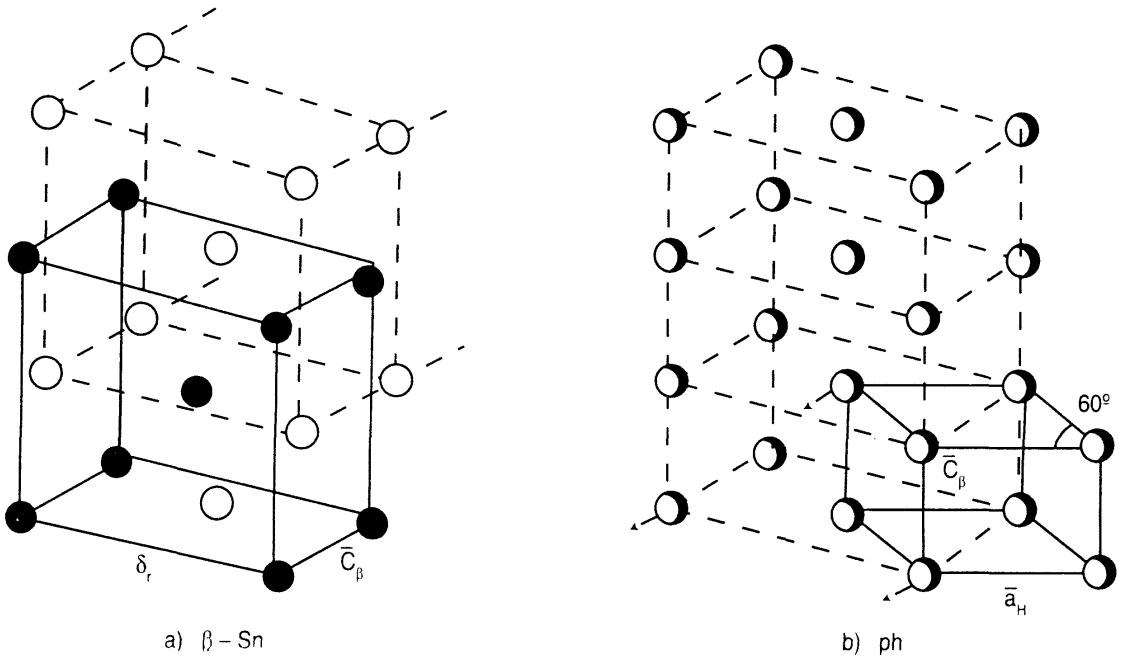

Fig 20 Structural relationship between ph and β-Sn structure

the C_β axis to give a base centred orthorhombic cell.

It was shown by Ivanov *et al.*[53] that the rare ph structure in Si was of low stability as there are a number of low frequency vibrational modes in it. Thus transformations to different structures from ph phase are expected. Indeed this has been observed on further application of pressures in Si as well in a few alloys where this phase can be stabilized at room pressure[54-56].

ph (Si) → Cmca(Si VI) → hcp

ph ($Sn_{0.75}$ $In_{0.25}$) → bct → hcp

ph ($Hg_{0.1}$ $Sn_{0.9}$) → bct → ?

Again there are structural relations between the ph and these various phases.

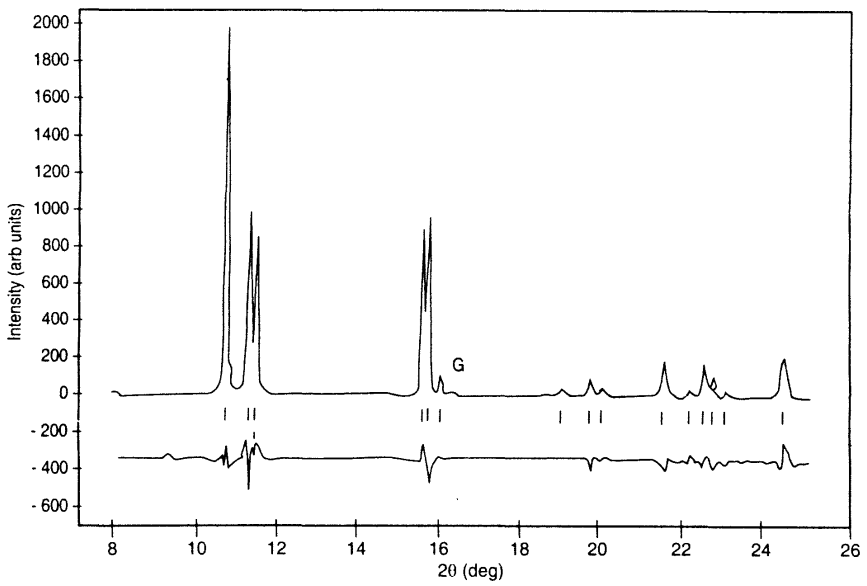

Fig. 21 A Reitveld fit to the experimental diffraction profile of Si at 13 Gpa using Imma structure. The tickmarks show the position of all reflections allowed by the symmetry. The diffrence between the observed and calculated profile is shown below the tickmarks. G represents a weak gasket line[52]

11 Conclusions

The applications described above show that in the recent years, use of high pressure X-ray crystallography has helped in deeper understanding of materials under high pressures. Particularly, synchrotron radiation sources have been used to investigate subtle phase transformations, low z materials and determination of physical properties such as equation of state, elastic properties etc., to pressures greater than at the centre of the earth. These careful and detailed experiments have in turn led to developments in theoretical capabilities resulting in an overall growth of deeper understanding of tunability of physical properties of substances with the help of high pressures.

12 Acknowledgement

The authors are grateful to Dr R Chidambaram for constant encouragement and several useful discussions. The authors also acknowledge many useful discussions with Dr B K Godwal.

References

1 A L Ruoff *High Press Res* **1** (1988) 1

2 H K Mao, R J Hemley and A L Mao *Advances in High Pressure Research in Condensed Matter* (Eds. S K Sikka, S C Gupta and B K Godwal) NISCOM: New Delhi (1997) p 12

3 H Olijnyk, S K Sikka and W B Holzapfel *Phys Lett* **A 103** (1984) 137

4 S M Sharma and S K Sikka *Prog Mater Science* **40** (1996) 1

5 S K Sikka, B K Godwal and R Chidambaram *High Pressure Shock Compression of Solids III* (Eds. Lee Davidson and M Shahinpoor) Springer: New York (1997) p 1

6 S K Sikka, Y K Vohra and R Chidambaram *Prog Mater Sci* **27** (1982) 245

7 U Benedict and W B Holzapfel *Handbook on the Physics and Chemistry of Rare Earths* (Eds. K A Gschneidner Jr., L Erying, G H Lander and G R Choppin) (North-Holland : Amsterdam) **17** (1993) p 245; *J Less Common Met* **100** (1984) 153

8 A Jayaraman *Rev Mod Phys* **55** (1983) 65

9 W B Holzapfel and W May *High Pressure Research in Geophysics* (Eds M H Manghnani and S I Akimoto) Reidel: Berlin (1982) p 73

10 S K Sikka, H Sankaran, S M Sharma, V Vijayakumar, B K Godwal and R Chidambaram *Ind Jl Pure & Appl Phys* **27** (1989) 472

11 R Chidambaram and S M Sharma *Bull Mater Sci* **22** (1999) 153

12 M Yousuf *Semiconductors and Semimetals* **55** (1998) 381

13 S Natrajan *et al. Proc AIRAPT-17* (to be published)

14 S C Gupta, J M Daswani, S K Sikka and R Chidambaram *Curr Sci* **65** (1993) 3999

15 V Vijayakumar *et al.* (Unpublished)

16 A B Garg, A Sinha, V Vijayakumar, B K Godwal and S K Sikka *Solid State Physics (India)* (1999) 42

17 H Sankaran, S K Sikka, S M Sharma and R Chidambaram *Phys Rev B* **38** (1988) 170

18 S L Chaplot and S K Sikka *Phys Rev B* **47** (1993) 5710

19 M S Somayazulu, S M Sharma, N Garg, S L Chaplot and S K Sikka *J Phys Cond Matter Phys* **65** (1993) 6345

20 J S Tse and D D Klug *Phys Rev Lett* **70** (1993) 174

21 M S Somayazulu, S M Sharma and S K Sikka *Phys Rev Lett* **73** (1994) 98

22 C Meade, R J Hemley and H K Mao *Phys Rev Lett* **69** (1992) 1387

23 Nandini Garg and S M Sharma *J Phys Cond Matt Phys* (Accepted)

24 M B Kruger and R Jeanloz *Science* **249** (1990) 647

25 H Sankaran, S M Sharma, S K Sikka and R Chidambaram *Pramana J Phys* **35** (1990) 177

26 P Gillet, J Badro, B Varrel and Paul F McMillan *Phys Rev* **B 51** (1955) 11262

27 N Garg, S M Sharma and S K Sikka *Solid State Physics* (India) **42** 1999

28 Nandini Garg *et al.* (to be published)

29 P Loubeyre *et al. Nature* (London) **383** (1996) 702

30 R J Hemley *et al. Nature* (London) **330** (1987) 737 R J Hemley, A F Goncharov, V V Struzhkin, Z Liu, J Shu and H K Mao *Proc AIRAPT-17 Conf* (1999) (To appear)

31 J P Amoureux M Bee and J C Damien *Acta Cryst* **B 36** (1980) 2633

32 T Ito *Acta Cryst* **B29** (1973) 364

33 S K Sikka and S M Sharma *Curr Sci* **63** (1992) 317

34 M A Rekha in *Advances in High Pressure Sci & Tech* IX NCST (1997) 182

35 V Vijayakumar, B K Godwal, A B Garg and S K Sikka *Solid State Physics (India)* **42** (1999) 180

36 R Chidambaram and S C Gupta *High Pressure Res* **12** (1994) 51

37 K J Kingma, R J Hemley, H K Mao and D R Veblen *Phys Rev Lett* **70** (1993) 3927 *Phys Rev Lett* **72** (1994) 1302

38 S Tsuneyuki, T Tsukada and H Aoki *Phys Rev Lett* **61** (1988) 869; S Tsuneyuki Y Matsui H Aoki and T Tsukada *Nature* (Lond) **339** (1989) 209

39 A K Singh, H K Mao, J Shu and R J Hemley *Phys Rev Lett* **80** (1998) 2157

40 H K Mao, J Shu, G Shen, R J Hemley, B Li and A K Singh *Nature* (Lond) **396** (1998) 741

41 A K Singh and C Balasingh *J Appl Phys* **75** (1994) 4956

42 O L Anderson *J Geophys Res* **95** (1990) 21697

43 S K Saxena, G Shen and P Lazar *Science* **260** (1993) 1312

44 S K Saxena, L S Dubrovinsky, P Haggkvist, Y Cerenius, G Shen and H K Mao *Science* **269** (1997) 1703

45 C S Yoo, J Akella, A J Campbell, H K Mao and R J Hemley *Science* **270** (1995) 1473

46 D Andrault, G Fiquet, M Kunz, F Visocekas and D Hausermann *Science* **278** (1997) 831

47 R S Rao, P Modak, B K Godwal and S K Sikka *Phys Rev* **B 59** (1999) 13498

48 G Shen, H Mao, R J Hemley, T S Duffy and M L Rivers *Geophys Res Lett* **25** (1998) 373

49 S J Duclos, Y K Vohra and A L Ruoff *Phys Rev Lett* **58** (1987) 775

50 Y K Vohra, K E Brister, S Desgreniers, A L Ruoff, K J Chang and M L Cohen *Phys Rev Lett* **56** (1986) 1944

51 S M Sharma and S K Sikka *J Phys Chem Solids* **46** (1985) 477

52 M I McMahon and R J Nelmes *Phys Rev* **B 47** (1993) 8337

53 A S Ivanov, A Yu Rumiantsev, N L Metrofanov and M Alba *Physica* **B 174** (1991) 79

54 M Hanfland, U-Schwarz, K Syassen and K Takemura *Phys Rev Lett* **82** (1999) 1197

55 S Meenakshi, V Vijayakumar, B K Godwal and S K Sikka *Solid State Physics* (India) **42** (1999) 178

56 V F Degtyareva, O Degtyareva, M Winzenick and W B Holzaptel *Phy Rev* **B59** (1999) 6058